Atom-Resonant Heralded Single Photons by "Interaction-Free Measurement"

Florian Wolfgramm, Yannick A. de Icaza Astiz, Federica A. Beduini, Alessandro Cerè, and Morgan W. Mitchell
ICFO - Institut de Ciencies Fotoniques, Mediterranean Technology Park, 08860 Castelldefels (Barcelona), Spain
(Dated: 1 February 2010)

We demonstrate the generation of rubidium-resonant heralded single photons for quantum memories. Photon pairs are created by cavity-enhanced down-conversion and narrowed in bandwidth to 7 MHz with a novel atom-based filter operating by "interaction-free measurement" principles. At least 94% of the heralded photons are atom-resonant as demonstrated by a direct absorption measurement with rubidium vapor. A heralded auto-correlation measurement shows $g_c^{(2)}(0) = 0.040 \pm 0.012$, i.e., suppression of multi-photon contributions by a factor of 25 relative to a coherent state. The generated heralded photons can readily be used in quantum memories and quantum networks.

PACS numbers: 42.50.Dv, 42.50.Ar, 42.65.Lm, 42.65.Yj

Introduction. - The availability of single photons is a crucial requirement in quantum information, quantum communication and quantum metrology. For quantum networks, the photons (*flying qubits*) should be resonant with atoms (*stationary qubits*) for storage and/or processing. For this reason, it has been an important goal of quantum optics to produce high-purity single photons capable of interaction with atoms. While there exist a number of different single-photon sources, most of these do not fulfill all necessary requirements [29]. The most widely used heralded single-photon source, spontaneous parametric down-conversion (SPDC) [1, 2], produces photons with a spectral width orders of magnitude larger than typical atomic natural linewidths. Passive filtering of SPDC photons is possible and has been demonstrated [3], but shows low count rates that are not sufficient for many tasks. Cavity-enhancement of the down-conversion process has established itself in recent years as a method to not only enhance the total photon rate, but at the same time to enhance the emission into the spectral and spatial modes of the cavity, producing high-purity photon states at high rates [4–11].

Bocquillon et al. [12] identify two critical figures of merit for heralded single-photon sources. The first, $g_{S,I}^{(2)}(\tau)$, describes the cross-correlation of signal and idler beams, a measure of reliability of the heralding mechanism. The second, $g_c^{(2)}(\tau)$, describes the conditional auto-correlation of the signal beam, a measure of the single-photon character of the heralded state. $g_c^{(2)}(0) < 1$ indicates non-classical behavior; $g_c^{(2)}(0) = 0$ for an ideal source.

Experiments using a cavity-enhanced, but unfiltered, source [11] have demonstrated $g^{(2)}(0) < 1$, but work in a regime where many longitudinal frequency modes, spread over tens of GHz, contribute to the signal. A cavity-enhanced source with optical-cavity filtering of the heralding (idler) beam and homodyne detection of the signal produced highly non-classical states: 70% of the heralded pulses contained a single photon in the mode to which the detection was sensitive [6, 7]. Undetected modes, however, contained photons spread over a large bandwidth. A recent experiment reports nearly 10% efficient atom-storage of beams from filtered cavity-enhanced SPDC, implying at least 10% atom-resonance, but made no measurement of $g_c^{(2)}(0)$ [13]. To date, no SPDC single-photon source has demonstrated atom-resonance of more than a small fraction of its output.

Here we demonstrate the generation of atom-resonant heralded single photons with high spectral purity: within the detection window of 400-1000 nm (450 THz), at least 94% of the photons are in a single, 7 MHz-bandwidth mode at the D_1 line of ^{87}Rb. Multi-photon contamination is at most 4%. We achieve this using an atom-based filter, inspired by the "interaction-free measurement" (IFM) strategy of Elitzur and Vaidman [14] (also known as "quantum interrogation" [15]). The IFM proposal is based on a balanced Mach-Zehnder interferometer in which due to destructive interference one of the two output ports is dark. The presence of an opaque object in either interferometer arm changes the interference and thus increases the probability of a photon exiting through the dark port. In our filtering scheme the object is a hot atomic vapor which is opaque at the transition frequencies. This guarantees the frequency of photons exiting through the dark port to be at an atomic transition.

IFM experiments have been proposed and demonstrated in different systems [16] and for a variety of applications including imaging [17] and quantum computing [18–20]. Intrinsic stability and intrinsic atom-resonance make our system robust and attractive for quantum networking applications. Our IFM filtering technique could be used also with solid-state ensembles [21, 22].

Experimental setup. - The experiment combines a cavity-enhanced down-conversion source locked to a rubidium transition, described in detail in [9, 23] and an intrinsically atom-resonant narrow-band filter, described in [24]. The setup is shown schematically in Fig. 1.

A single-frequency diode laser is locked to the $5^2S_{1/2}(F=2) \rightarrow 5^2P_{1/2}(F'=1)$ transition of the D_1 line of ^{87}Rb. Part of the laser output is frequency dou-

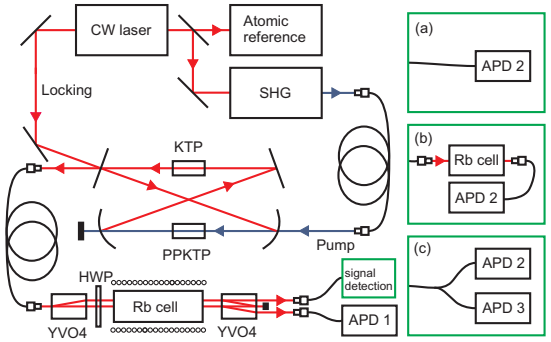

FIG. 1: Experimental setup. SHG, second harmonic generation cavity; PPKTP, phase-matched nonlinear crystal; KTP, compensating crystal; YVO4, Yttrium Vanadate crystal; HWP, half wave plate; APD, avalanche photo-diode. (a)-(c), different measurement scenarios for the signal photon detection.

bled and pumps the cavity-enhanced down-conversion system at a typical pump power of 25 mW. Type-II phase-matched down conversion takes place in a 2 cm-long phase-matched periodically poled potassium titanyl phosphate (PPKTP) crystal. Another KTP crystal (neither pumped nor phase-matched) inside the cavity is temperature tuned to achieve simultaneous resonance of signal and idler modes. The type-II process generates photon pairs with mutually perpendicular polarizations. This allows for straightforward separation of signal and idler photon and also for easy generation of polarization entanglement. A locking beam from the same diode laser, and therefore also at the same rubidium transition frequency, is used to stabilize the cavity length. In this way, we guarantee the presence of frequency-degenerate cavity modes at the atomic transition frequency. After leaving the cavity, the generated photon pairs are coupled into a single-mode fiber.

The pumped, nonlinear cavity acts as a sub-threshold optical parametric oscillator and generates resonant pairs of modes. With the cavity locked and doubly-resonant for signal and idler modes, the output spectrum is determined by the 148 GHz phase-matching bandwidth of the down-conversion process. Within this envelope the spectrum consists of hundreds of non-degenerate frequency modes spaced by the free spectral range of 490 MHz, centered around the degenerate mode at the rubidium transition frequency.

To achieve filtering that guarantees a high ratio between degenerate and non-degenerate modes, e.g., a signal-to-noise ratio of 90%, requires an extinction ratio of several thousand, over a bandwidth of hundreds of GHz. In principle this filtering can be achieved with optical cavities. Consecutive cavities with incommensurate free spectral ranges have been used in other experiments [3, 6, 7], but do not appear to reach high rejection ratios. Neergaard-Nielsen et al. report a 20% discrepancy in effective signal detection efficiency, and give "insufficient suppression of uncorrelated frequency modes in the series of trigger filters" as a likely explanation [7]. A small misalignment or aberration would be sufficient to couple into higher modes and spoil the extinction ratio.

In contrast, our filter operates by principles of "interaction-free measurement" [14, 25] and combines extremely broadband optics (birefringent polarizers) with extremely narrow-band optics (atoms) with a large angular acceptance, thus practically insensitive to mode misalignment.

As shown in Fig. 1, a YVO_4 crystal separates horizontally and vertically polarized photons by 1 mm. The polarization modes travel parallel to each other through a hot rubidium cell of isotopically pure ^{87}Rb, optically pumped by a single-frequency laser resonant to the F=2→F'=3 transition of the D_2 line of ^{87}Rb (not shown). Due to Doppler shifts, the optical pumping only effects a portion of the thermal velocity distribution, and creates a circular dichroism with a sub-Doppler linewidth of about 80 MHz. A second YVO_4 crystal introduces a second relative displacement, which can re-combine or further separate the photons, depending on polarization. Separated photons are collected, while re-combined photons are blocked. A half wave plate is used to switch between the "active" configuration, in which only photons that change polarization in the cell are collected, and the "inactive" configuration, in which photons that do not change are collected. In the "active" configuration, the system acts as an IFM detector for polarized atoms: a photon is collected only if it experiences a polarization change, i.e., if it is resonant with the optically pumped atoms, which absorb one circular component of the photon polarization state. Neighboring modes of the degenerate mode at the rubidium transition are already 490 MHz detuned and therefore outside of the filter linewidth of 80 MHz. The out-of-band extinction ratio is $\geq$35 dB. The filter transmission is optimized by adjusting the overlap between pump and single-photon mode, the rubidium vapor temperature and the magnitude of a small orienting applied magnetic field. The temperature is set to 65°C, which corresponds to an atomic density of $5 \cdot 10^{11}$ cm^{-3}. The measured filter transmission of 10.0% for horizontal polarization and 9.5% for vertical polarization is limited by pump power and in principle can reach 25% [24]. To avoid contamination of the single-photon mode by scattered pump light, the pump enters the vapor cell at a small angle and counter-propagating to the single-photon mode. Interference filters centered on 795 nm further reject the 780 nm pump light with an extinction ratio of $>10^5$. The measured contribution from pump photons is below the detectors' dark count rate. Each output is coupled into single-mode fiber. One is detected directly on a fiber-coupled avalanche photo diode (APD, Perkin Elmer SPCM-AQ4C). The other is used for subsequent experiments. Photon detections are

recorded by a counting board (FAST ComTec P7888) for later analysis.

Time-correlation measurements. - First, the time distribution of the difference in arrival time between signal and idler photons is analyzed in absence of the filter (Fig. 1(a)). We follow the theory developed in [2, 11, 12, 26]. The cross-correlation function between signal and idler modes is

$$g^{(2)}_{S,I}(\tau) \equiv \frac{\langle E^\dagger_S(t+\tau)E^\dagger_I(t)E_I(t)E_S(t+\tau)\rangle}{\langle E^\dagger_I(t)E_I(t)\rangle\langle E^\dagger_S(t+\tau)E_S(t+\tau)\rangle}, \qquad (1)$$

where $E_{S,I}$ are the operators of the signal and idler fields. In the case of doubly-resonant cavity-enhanced down-conversion it takes this form:

$$g^{(2)}_{S,I}(\tau) \propto \left| \sum_{m_S,m_I=0}^{\infty} \frac{\sqrt{\gamma_S\,\gamma_I\,\omega_S\,\omega_I}}{\Gamma_S+\Gamma_I} \times \begin{cases} e^{-2\pi\Gamma_S(\tau-(\tau_0/2))}\mathrm{sinc}(i\pi\tau_0\Gamma_S) & \tau \geqslant \frac{\tau_0}{2} \\ e^{+2\pi\Gamma_I(\tau-(\tau_0/2))}\mathrm{sinc}(i\pi\tau_0\Gamma_I) & \tau < \frac{\tau_0}{2} \end{cases} \right|^2, \qquad (2)$$

where $\gamma_{S,I}$ are the cavity damping rates for signal (S) and idler (I), $\omega_{S,I}$ are the central frequencies, τ_0 is difference between the transit times of a signal and idler photon through the SPDC crystal, $\Gamma_{S,I} \equiv \gamma_{S,I}/2 + im_{S,I}\Delta\omega_{S,I}$ with mode indices $m_{S,I}$ and free spectral ranges $\Delta\omega_{S,I}$ [11, 26]. Due to compensation, $\Delta\omega_S = \Delta\omega_I \equiv \Delta\omega$ in our cavity.

We first measure the $g^{(2)}_{S,I}(\tau)$-function with the filter in the "inactive" configuration at a much reduced pump power. The histogram of the difference in arrival time between detection events in the two APDs is shown in Fig. 2. The blue bars represent the coincidence event detections within time bins of 1 ns, the resolution of the counting board. The black bars, drawn inverted for better visibility, show the theoretical prediction based on Eq. (2). The height of the theory histogram, the only free parameter, has been set to match the height of the data. Experimental and theoretical results are in excellent agreement. The comb-like structure of the histogram is a consequence of interference between different frequency modes. The temporal spacing between neighboring peaks corresponds to the cavity round-trip time $1/\Delta\omega \approx 2.04$ ns.

When the filter is "active", the arrival time difference histogram shows a smooth double-exponential shape, without multi-mode interference (Fig. 3). This already indicates that only a single frequency mode is transmitted through the filter. The theory (lower black bars) is given by Eq. (2) for a single mode ($\Gamma_{S,I}$=$\gamma_{S,I}/2$). The data shows a very low background noise level. Throughout, raw data are shown; background coincidences have not been subtracted.

In this experiment we are interested in time correlations, but it is interesting to ask if other kinds of correlations and possible entanglement, e.g. in polarization or in frequency, are also preserved by the filter. By design, the filter should transmit nearly equally different frequency and polarization components of the selected cavity mode, preserving correlations: absorptive and refractive effects vary on the scale of the 80 MHz absorption linewidth, large relative to the 7 MHz of the cavity mode. Also, the axial magnetic field scrambles any linear birefringence or dichroism, giving equal response for the two linear polarizations. Preliminary results indicate that the degree of polarization as well as the entanglement in a polarization entangled state are not changed significantly by the filter. A detailed study of this will be the subject of a future publication.

Atom-resonance. - To measure the atom-resonant frac-

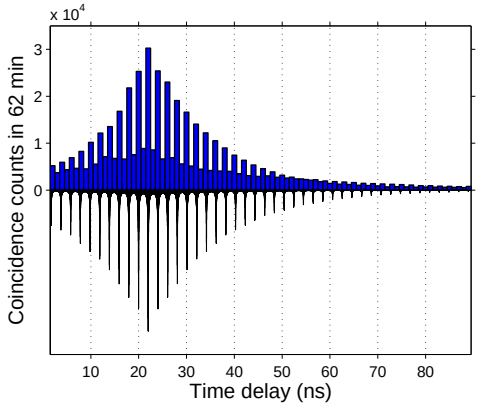

FIG. 2: Arrival time histogram of unfiltered photon pairs; experimental data (upper bars) and theory (lower bars). The frequency-comb structure is reflected by a comb-like structure in the temporal domain. The visibility of the experimental data is limited by time resolution of the counting electronics.

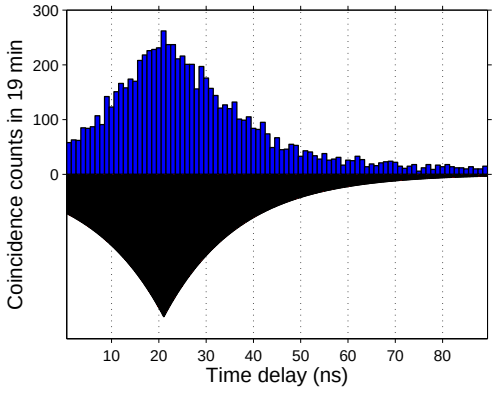

FIG. 3: Arrival time histogram of filtered photon pairs; experimental data (upper bars) and theory (lower bars). The disappearance of the comb structure in the filtered case indicates the single-mode character of the filtered fields.

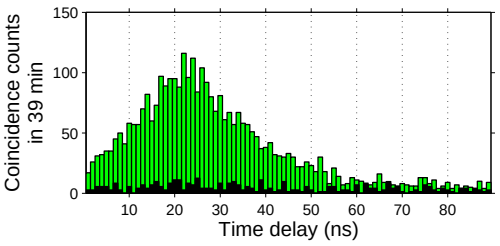

FIG. 4: Arrival time histogram of filtered photon pairs after passing the signal photons through a rubidium vapor cell at an optical density of 0.3 (upper green bars) and at an optical density of 6 (lower black bars).

tion, we let the filtered photons of the signal arm propagate through a rubidium vapor cell (Fig. 1(b)). At room temperature, the cell's optical density (OD) is low (0.3) corresponding to a transmission of 74% and coincidences between the detection events on the two APDs are observed (Fig. 4, upper green bars). By heating the rubidium cell, an optical density of 6, or 0.25% resonant transmission, is reached. The coincidences drop to the background level (Fig. 4, lower black bars). Within a coincidence window of 40 ns, the ratio of raw OD 0.3 coincidences to raw OD 6 coincidences is 11.6:1, indicating rubidium resonance of at least 94% of the photons.

Suppression of multi-photon events. - The signal autocorrelation function, given a trigger detection of the idler, is [2, 11, 12]

$$g_c^{(2)}(\tau) = \frac{\langle E_S^\dagger(t+\tau)E_S^\dagger(t)E_S(t)E_S(t+\tau)\rangle}{\langle E_S^\dagger(t)E_S(t)\rangle\langle E_S^\dagger(t+\tau)E_S(t+\tau)\rangle}. \qquad (3)$$

The crucial figure of merit is the value of the autocorrelation function of signal photons $g_c^{(2)}(\tau)$ at $\tau = 0$. We measure $g_c^{(2)}(0)$ as follows: the signal mode is split by a 50/50 beam splitting fiber and the coincidences between the idler detector (APD1) and the two signal detectors (APD2 and APD3) are analyzed (Fig. 1(c)). The detection of an idler photon defines a coincidence window of 40 ns, symmetrical around the detection time. Individual and coincident detections in this time window give singles counts N_2, N_3, while detections at both APD2 and APD3 give the coincidence count N_{23}. N_{23} corresponds to unwanted multi-photon contributions which are very low in our experiment. To accurately estimate N_{23}, we measure for large coincidence windows of up to 2000 ns, extrapolate down to 40 ns, and multiply by two, to account for possible bunching [11, 12]. We then calculate

$$g_c^{(2)}(0) \approx \frac{N_{23}N_1}{N_2N_3}, \qquad (4)$$

where N_1 is the number of idler trigger events [1, 2, 12]. We note that this gives an upper limit for $g_c^{(2)}(0)$, due to the conservative bunching factor and the finite time window. We find $g_c^{(2)}(0) \leq 0.040 \pm 0.012$, 80 standard deviations below the classical limit of 1.

Summary. - Using an ultra-bright cavity-enhanced down-conversion source and an atom-based filter operating by "interaction-free measurement" principles, we have generated for the first time narrow-band, high-spectral purity, atom-resonant heralded single photons from SPDC. Of the generated photons, 94% are resonant to a rubidium transition frequency. A $g_c^{(2)}$-measurement shows an upper limit of $g_c^{(2)}(0) = 0.040 \pm 0.012$ corresponding to a reduction of multiple photon events by a factor of at least 25 compared to a coherent state. The source is an ideal tool for atom-photon interactions at the single-photon level, for quantum memories in EIT media [27] and solid-state systems [21, 22] and single-photon single-atom interfaces [3, 28].

We acknowledge useful discussions with P. Kwiat, H. de Riedmatten and C. Vitelli. This work was supported by the Spanish Ministry of Science and Innovation under the Consolider-Ingenio 2010 Project "Quantum Optical Information Technologies" and the ILUMA project (No. FIS2008-01051) and by an ICFO-OCE collaborative research program. F. W. is supported by the Commission for Universities and Research of the Department of Innovation, Universities and Enterprises of the Catalan Government and the European Social Fund.

[1] P. Grangier, G. Roger, and A. Aspect, Europhys. Lett. **1**, 173 (1986).
[2] S. Fasel *et al.*, New J. Phys. **6**, 163 (2004).
[3] N. Piro *et al.*, Nat Phys, doi:10.1038/nphys1805, (2010).
[4] Z. Y. Ou and Y. J. Lu, Phys. Rev. Lett. **83**, 2556 (1999).
[5] C. E. Kuklewicz, F. N. C. Wong, and J. H. Shapiro, Phys. Rev. Lett. **97**, 223601 (2006).
[6] J. S. Neergaard-Nielsen *et al.*, Phys. Rev. Lett. **97**, 083604 (2006).
[7] J. S. Neergaard-Nielsen *et al.*, Opt. Express **15**, 7940 (2007).
[8] M. Scholz *et al.*, Appl. Phys. Lett. **91**, 191104 (2007).
[9] F. Wolfgramm *et al.*, Opt. Express **16**, 18145 (2008).
[10] X.-H. Bao *et al.*, Phys. Rev. Lett. **101**, 190501 (2008).
[11] M. Scholz, L. Koch, and O. Benson, Phys. Rev. Lett. **102**, 063603 (2009).
[12] E. Bocquillon *et al.*, Phys. Rev. A **79**, 035801 (2009).
[13] X.-M. Jin *et al.*, arXiv:quant-ph/1004.4691.
[14] A. Elitzur and L. Vaidman, Found. Phys. **23**, 987 (1993).
[15] P. G. Kwiat *et al.*, Phys. Rev. Lett. **83**, 4725 (1999).
[16] G. S. Paraoanu, Phys. Rev. Lett. **97**, 180406 (2006).
[17] A. G. White *et al.*, Phys. Rev. A **58**, 605 (1998).
[18] O. Hosten *et al.*, Nature **439**, 949 (2006).
[19] G. Mitchison and R. Jozsa, arXiv:quant-ph/0606092.
[20] L. Vaidman, Phys. Rev. Lett. **98**, 160403 (2007).
[21] H. de Riedmatten *et al.*, Nature (London) **456**, 773 (2008).
[22] M. P. Hedges *et al.*, Nature **465**, 1052 (2010).
[23] F. Wolfgramm, A. Cerè, and M. W. Mitchell, J. Opt.

Soc. Am. B **27**, A25 (2010).
[24] A. Cerè *et al.*, Opt. Lett. **34**, 1012 (2009).
[25] P. Kwiat *et al.*, Phys. Rev. Lett. **74**, 4763 (1995).
[26] U. Herzog, M. Scholz, and O. Benson, Phys. Rev. A **77**, 023826 (2008).
[27] M. D. Eisaman *et al.*, Nature (London) **438**, 837 (2005).
[28] M. K. Tey *et al.*, Nature Phys. **4**, 924 (2008).
[29] A review of narrow-band generation methods and their limitations is provided in Reference [7]